

---

# Neurosymbolic Grounding for Compositional World Models

---

Atharva Sehgal  
UT Austin

Arya Grayeli  
UT Austin

Jennifer J. Sun  
Caltech

Swarat Chaudhuri  
UT Austin

<https://trishullab.github.io/cosmos-web>

## Abstract

We introduce COSMOS, a framework for object-centric world modeling that is designed for compositional generalization (CG), i.e., high performance on unseen input scenes obtained through the composition of known visual “atoms.” The central insight behind COSMOS is the use of a novel form of neurosymbolic grounding. Specifically, the framework introduces two new tools: (i) neurosymbolic scene encodings, which represent each entity in a scene using a real vector computed using a neural encoder, as well as a vector of composable symbols describing attributes of the entity, and (ii) a neurosymbolic attention mechanism that binds these entities to learned rules of interaction. COSMOS is end-to-end differentiable; also, unlike traditional neurosymbolic methods that require representations to be manually mapped to symbols, it computes an entity’s symbolic attributes using vision-language foundation models. Through an evaluation that considers two different forms of CG on an established blocks-pushing domain, we show that the framework establishes a new state-of-the-art for CG in world modeling.

## 1 Introduction

The discovery of world models — deep generative models that predict the outcome of an action in a scene made of interacting entities — is a central challenge in contemporary machine learning [12, 13]. As such models are naturally factorized by objects, methods for learning them [10, 21, 40, 44] commonly follow a modular, object-centric perspective. Given a scene represented as pixels, these methods first extract representations of the entities in the scene, then apply a transition network to model interactions between the entities. The entity extractor and the transition model form an end-to-end differentiable pipeline.

Of particular interest in world modeling is the property of *compositional generalization* (CG), i.e., test-time generalization to scenes that are novel compositions of known visual “atoms”. Recently, [44] gave a first approach to learning world models that compositionally generalize. Their method uses an *action attention* mechanism to bind actions to entities. The mechanism is designed to be equivariant to the replacement of objects in a scene by other objects, enabling CG.

This paper continues the study of world models and CG. We note that CG is hard for purely neural methods, as they cannot easily learn encodings that can be decomposed into well-defined parts. Our approach, COSMOS, uses a novel form of *neurosymbolic grounding* to address this issue.

The centerpiece idea in COSMOS is the notion of *object-centric, neurosymbolic scene encodings*. Like in prior modular approaches to world modeling, we extract a discrete set of entity representations from an input scene. However, each of these representations consists of: (i) a standard real vector representation constructed using a neural encoder, and (ii) a vector of *symbolic attributes*, capturing important properties — for example, shape, color, and orientation — of the entity.

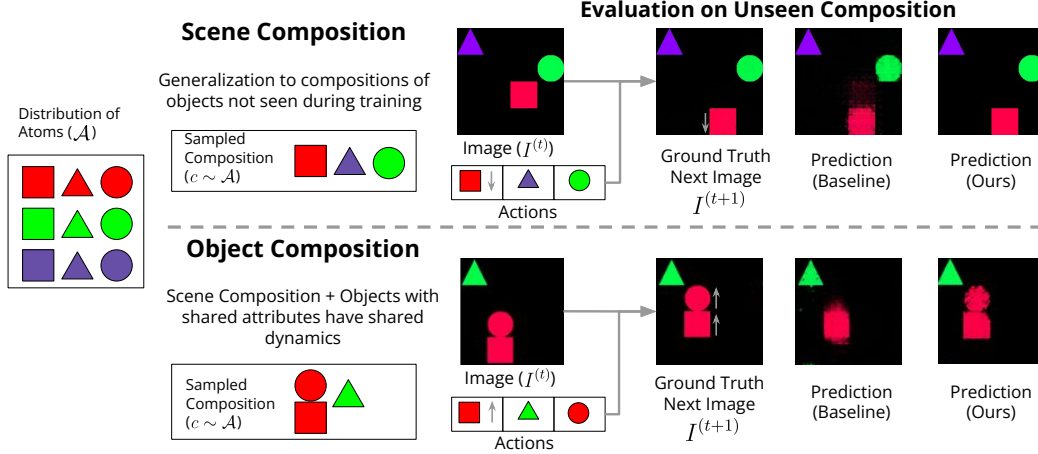


Figure 1: Overview of compositional world modeling. We depict examples from a 2D block pushing domain consisting of shapes that interact, where we can generate samples of different shapes and interactions. We aim to learn a model that generalizes to compositions not seen during training, such as scene composition (*top*) and object composition (*bottom*). Previous works [9] focus on scene composition, and struggle to generalize to harder compositional environments. Our approach COSMOS leverages object-centric, neurosymbolic scene encodings to compositionally generalize across settings containing different types of compositions.

Like [10], we model transitions in the world as a collection of neural modules, each capturing a “rule” for pairwise interaction between entities. The mechanism for binding these rules to the entities is based on a novel *neurosymbolic attention* mechanism, in which the keys are symbolic, and the queries are neural. The symbolic keys are matched with the symbolic components of the entity encodings, enabling decisions such as “the  $i$ -th rule represents interactions between a black object and a circular object” (here, “black” and “circular” are symbolic attributes). The rules, the attention mechanism, and the entity extractor constitute an end-to-end differentiable pipeline.

The CG abilities of this model stems from the compositional nature of the symbolic attributes. The symbols naturally capture “parts” of scenes. The neurosymbolic attention mechanism fires rules based on (soft, neurally represented) logical conditions over the symbols and can cover new compositions of the parts.

A traditional issue with neurosymbolic methods for perception is that they need a human-provided mapping between perceptual inputs and their symbolic attributes [14, 32]. However, COSMOS automatically obtains this mapping from vision-language foundation models. Concretely, to compute the symbolic attributes of an object, we utilize CLIP [27] to assign each object values from a set of known attributes.

We compare COSMOS against a state-of-the-art baseline and an ablation on an established domain of moving 2D shapes [21]. Our evaluation considers two definitions of CG, illustrated in Figure 1. In one of these, we want the model to generalize to new *scene compositions*, i.e., input scenes comprising sets of entities that have been seen during training, but never together. The other definition, *object composition*, is new to this paper: here, we additionally need to accommodate shared dynamics between objects with shared attributes (e.g., the color red). Our results show that COSMOS outperforms the competing approaches at next-state prediction (Figure 1 visualizes a representative sample) and separability of the computed latent representations, as well as accuracy in a downstream planning task. Collectively, the results establish COSMOS as a state-of-the-art for CG world modeling.

To summarize our contributions, we offer: (i) COSMOS, the first neurosymbolic, end-to-end differentiable approach — based on a combination of neurosymbolic scene encodings and neurosymbolic attention — to object-centric world modeling. (ii) a new way to use foundation models to automate symbol construction in neurosymbolic learning; (iii) an evaluation that shows COSMOS to produce significant empirical gains over the state-of-the-art for CG world modeling.

## 2 Problem Statement

We are interested in learning world models that compositionally generalize. World models arise naturally out of the formalism for Markov decision processes (MDPs). An MDP  $\mathcal{M}$  is defined by a 5 tuple  $(\mathcal{S}, \mathcal{A}, T, R, \gamma)$  with state space  $\mathcal{S}$ , action space  $\mathcal{A}$ , transition function  $T : \mathcal{S} \times \mathcal{A} \rightarrow \mathcal{S} \times \mathbb{R}_{\geq 0}$ , immediate reward function  $R : \mathcal{S} \times \mathcal{A} \rightarrow \mathbb{R}$ , and discount factor  $\gamma \in [0, 1]$ . We make three additional constraints:

**Object-Oriented state and action space:** In our environments, the state space is realized as images. At each time step  $t$ , an agent observes an image  $I \in \mathcal{S}_{pixel}$  and takes an action  $A \in \mathcal{A}$ . However, learning  $\mathcal{S}_{pixel}$  directly is an intractable problem. Instead, we assume that the high dimensional state space can be decomposed into a lower dimensional *object-oriented* state space  $\mathcal{S} = \mathcal{S}_1 \times \dots \times \mathcal{S}_k$  where  $k$  is the number of objects in the image. Now, each *factor*  $S_i \in \mathcal{S}_i$  describes a single object in the image. Hence, the transition function has signature  $T : (S_1; A_1 \times \dots \times S_k; A_k) \rightarrow (S_1 \times \dots \times S_k)$  where each factor  $A_i$  is a factorized set of actions associated with object representation  $S_i$  and  $(\circ; \circ)$  is the concatenation operator. A pixel grounding function  $P_{\downarrow} : \mathcal{S} \rightarrow \mathcal{S}_{pixel}$  enables grounding a factored state into an image.

**Symbolic object relations:** We assume that objects in the state space share attributes. An attribute is a set of unique symbols  $C_p = \{C_p^1, \dots, C_p^q\}$ . For instance, in the 2D block pushing domain (illustrated in Figure 1), each object has a “color” attribute that can take on values  $C_{color} := \{\text{red}, \text{green}, \dots\}$ . An object can be composed of many such attributes that can be retrieved using an attribute projection function  $\alpha_{\uparrow} : S_i \rightarrow \Lambda_i := (\Lambda_i^{C_1}; \dots; \Lambda_i^{C_p})$  where  $(C_1, \dots, C_p)$  is a predefined, ordered list of attributes and  $\Lambda_i^{C_p}$  selects the value in the  $C_p$ -th attribute that is most relevant to  $S_i$ . Note that  $\alpha_{\uparrow}$  only depends on a single object and trivially generalizes to different compositions of objects [20].

**Compositional Generalization:** To formalize CG, we first formalize compositions. We assume that each state in our MDP can be decomposed using two sets of elements: compounds and atoms. *Compounds* are sets of elements that can be decomposed into smaller sets of elements, and *atoms* are sets of elements that cannot be decomposed further. For instance, in the block pushing domain (Figure 1), we can designate each unique object as an atom and designate the co-occurrence of a set of atoms in a scene as a compound. We use  $\mathbf{A}$  to denote the elements designated to be the atoms and  $\mathbf{C}$  to denote the compounds. The frequency distribution of the atoms is  $\mathcal{F}_{\mathbf{A}}(\mathcal{D})$  and the frequency distribution of the compositions is  $\mathcal{F}_{\mathbf{C}}(\mathcal{D})$ . Given this, compositional generalization is expressed as a property of the train distribution  $\mathcal{D}_{train}$  and of the test distribution  $\mathcal{D}_{test}$  undergoing a distributional shift of the compounds, while the distribution of atoms remains the same.

Given the following assumptions, for any experience buffer  $\mathcal{D} := \{\{I^{(t)}, A^{(t)}\}_{t=1}^T \subseteq \mathcal{S}_{pixel} \times \mathcal{A}\}_{i=1}^N$ , learning a world model boils down to learning the transition function  $T$  for the MDP using the sequences of observations collected by  $\mathcal{D}$ . Specifically, for  $I^{(i,t)}, A^{(i,t)}, I^{(i,t+1)} \in \mathcal{D}$ , our objective function is

$$\mathcal{L} = \frac{1}{N(T-1)} \sum_{i=1}^N \sum_{t=1}^{T-1} \|P_{\downarrow} \left( T \left( S_1^{(i,t)}; A_1^{(i,t)} \dots, S_k^{(i,t)}; A_k^{(i,t)} \right) \right) - I^{(i,t+1)} \|_2^2$$

We study two kinds of compositions:

**Scene Composition:** Figure 1 shows an instance of scene centric CG in the block pushing domain. Here, there exist  $n = 9$  unique objects, but only  $k = 3$  are allowed to co-occur in any given realized scene. Each unique object represents an atom, and the co-occurrence of a set of  $k$  atoms in a scene represents the compound. Hence, there are a total  $\binom{n}{k}$  possible compositions. The distribution of atoms in the train distribution and the test distribution does not change, while the distribution of compounds at train time and at test time are disjoint. So,  $\mathcal{F}_{\mathbf{A}}(\mathcal{D}_{eval})$  is equivalent to  $\mathcal{F}_{\mathbf{A}}(\mathcal{D}_{train})$  while  $\mathcal{F}_{\mathbf{C}}(\mathcal{D}_{eval}) \cap \mathcal{F}_{\mathbf{C}}(\mathcal{D}_{train}) = \emptyset$ .

**Object Composition:** Figure 1 shows an instance of object composition in the block pushing domain. Here, there are  $n = 9, k = 3$  unique objects. A composition of objects occurs when two objects share attributes (for instance, here, the shared attributes are color and adjacency). Objects with shared attributes share dynamics. As a result, if one object experiences a force, others with the same attributes also undergo that force. Hence, assuming a single composition per scene, there are a

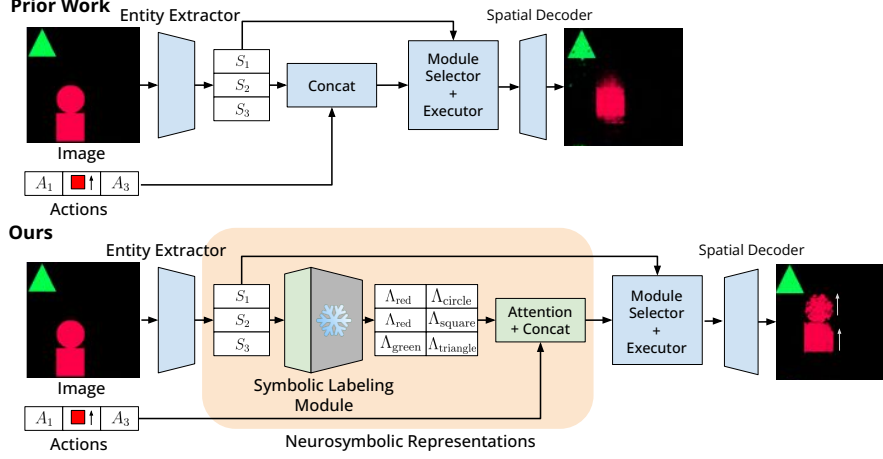


Figure 2: Comparing world modeling frameworks between prior work [9] and COSMOS. Both modules start with entity extraction, to obtain neural object representations  $\{S_1, S_2, S_k\}$  from the image (Section 3.1). While prior work uses this representation directly for the module selector, our work leverages a symbolic labeling module, which outputs a set of attributes  $\Lambda$ , to learn neurosymbolic representations (Section 3.2). We then perform action conditioning (Section 3.2.1) to keep track of corresponding actions, and update through a transition model (Section 3.3).

total  $\binom{n}{k} \binom{k}{2}$  possible compositions. As in the previous case,  $\mathcal{F}_A(\mathcal{D}_{eval})$  is equivalent to  $\mathcal{F}_A(\mathcal{D}_{train})$  while  $\mathcal{F}_C(\mathcal{D}_{eval}) \cap \mathcal{F}_C(\mathcal{D}_{eval}) = \emptyset$ .

### 3 Method

We approach neurosymbolic world modeling through object-centric neurosymbolic representations (Figure 2). Our method consists of: extracting object-centric encodings (Section 3.1), representing each object using neural and symbolic attributes (Section 3.2), and learning a transition model to update to next state (Section 3.3). Similar to previous works, we use slot based autoencoders to extract objects, but use symbolic grounding from foundation models alongside neural representations, which enables our model to achieve both scene and object compositionality. The full algorithm is presented in Algorithm 1, and the model is visualized in Figure 3.

**Algorithm 1** Neurosymbolic world model for  $k$ -factorized state space. The input is an image  $I$  of dimensions  $(C, H, W) = (3 \times 224 \times 224)$  and a set of  $k$ -factorized actions of dimension  $(k \times d_{action})$ . The model is trained end-to-end except for the SLM modules, whose weights are held constant. There are three global variables:  $T$ ,  $\{C_1, C_2, C_p\}$  and  $\{\vec{R}_1, \vec{R}_2, \vec{R}_l\}$ .  $T$  is the threshold of the number of repeated slot update steps,  $\{C_1, C_2, C_p\}$  denotes text encodings for the closed vocabulary and  $\{\vec{R}_1, \vec{R}_2, \vec{R}_l\}$  are learnable rule encodings.

---

```

1: function TRANSITIONIMAGE( $I, [A_1, A_2, A_k]$ )
2:    $\{S_1, S_2, S_k\} \leftarrow \text{ENTITYEXTRACTOR}(I)$   $\triangleright S_i$  dim:  $(k, d_{slot})$ 
3:   for  $i$  in range( $T$ ) do
4:      $\{I'_1, I'_2, I'_k\}, \{M'_1, M'_2, M'_k\} \leftarrow \text{SPATIALDECODER}(\{S_1, S_2, S_k\})$   $\triangleright I_i$  dim:  $(k, C, H, W)$ 
5:      $\{I_1, I_2, I_k\} \leftarrow \{M_i \cdot I'_i, \forall i \in [1, k]\}$ 
6:      $\{\Lambda_1, \Lambda_2, \Lambda_k\} \leftarrow \{\text{SLM}(I_i, \{C_1, C_2, C_p\}) | \forall i \in [1, k]\}$   $\triangleright$  dim:  $(k, p)$ 
7:      $\{\bar{\Lambda}_1, \bar{\Lambda}_2, \bar{\Lambda}_k\} \leftarrow \text{ACTIONATTN}(\{\Lambda_1, \Lambda_2, \Lambda_k\}, [A_1, A_2, A_k])$ 
8:      $p, c, r \leftarrow \text{MODULARRULENET}(\mathbf{K}=\{\bar{\Lambda}_1, \bar{\Lambda}_2, \bar{\Lambda}_k\}, \mathbf{Q}=\{\vec{R}_1, \vec{R}_2, \vec{R}_l\})$ 
9:      $S_p \leftarrow S_p + \text{MLPBANK}[r](\text{concat}(S_p, S_c, \vec{R}_r))$ 
10:     $\{I'_1, I'_2, I'_k\}, \{M'_1, M'_2, M'_k\} \leftarrow \text{SPATIALDECODER}(\{S_1, S_2, S_k\})$   $\triangleright I_i$  dim:  $(k, C, H, W)$ 
11:  return  $\sum_{i=1}^k M'_i \cdot I'_i$ 

```

---

### 3.1 Slot-based Autoencoder

An autoencoder transforms an image into a hidden representation and then reconstructs the image from this representation. We use a slot-based autoencoder to learn a factorized hidden representation, where each factor represents a single entity. Such autoencoder make two assumptions: (1) each factor captures a specific property of the image, and (2) collectively, all factors describe the entire input image. This set-structured representation enables unsupervised disentanglement of objects into individual entities. Our slot based autoencoder consists of two components:

**ENTITYEXTRACTOR** :  $I \rightarrow \{S_1, \dots, S_k\}$ : The entity extractor takes an image and produces a set-structured hidden representation describing each object. [23] introduce an iterative-refining based attention algorithm to learn such an encoding (slot attention). In our domains, slot attention and derivate works [5, 18] struggle to disentangle images into separate slots. To avoid the perception model becoming a bottleneck for studying dynamics learning, we propose a new entity extractor that uses Segment Anything [22] with pretrained weights to produce set-structured segmentation masks to decompose the image into objects and a Resnet-18 image encoder [15] to produce a set-structured hidden representation for each object. This model allows us to perfectly match ground truth segmentations in our domains while preserving the assumptions of set structured hidden representations.

**SPATIALDECODER** :  $\{S_1, \dots, S_k\} \rightarrow \{I'_1, I'_2, I'_k\}, \{M_1, M_2, M_k\}$ : The slot decoder is a permutation equivariant network that decodes the set of slots back to the input image. We follow previous works [9, 23, 44] in using a spatial decoder [41] that decodes a given set of vectors  $\{S_1, \dots, S_k\}$  individually into a set of reconstructions  $\{I'_1, I'_2, I'_k\}$  and a set of masks  $\{M_1, \dots, M_k\}$ . The final image  $I$  is produced by taking the Hadamard product of each reconstruction and its corresponding mask and adding all the resulting images together. That is,  $I = \sum_{i=1}^k M_i \cdot I'_i$ .

### 3.2 Neurosymbolic encoding

To achieve robust CG in our setting, our representation must be resilient to both object and attribute compositions. The  $k$  slot-based encoding, by construction, generalizes to object replacement. For attribute compositions, however, it is essential to know the exact attributes to be targeted for CG. Given these attributes, we propose describing each entity with a composition of *symbol vectors*. Each symbol vector is associated with a single entity and attribute, allowing it to trivially generalize to different attributes compositions. Moreover, we can ensure a canonical ordering of the symbols, making downstream attention-based computations invariant to permutations of attributes. We'll next detail our method for generating these symbol vectors.

**SLM** :  $I_i \times \{C_1, C_2, C_p\} \rightarrow \Lambda_i := (\Lambda_i^{C_1}; \dots; \Lambda_i^{C_p})$ : The symbolic labelling module (SLM) processes an image and a predefined list of attributes. Assuming this list is comprehensive (though not exhaustive), the module employs a pretrained CLIP model to compute attention scores between the image features and each entity encoding. The resulting logits indicate the alignment between the image and each attribute. The attribute most aligned with the image is then identified using a straight-through Gumbel softmax [17]. The gumbel-softmax yields the index of the most likely value for each attribute as one-hot vectors, which are concatenated together to form a bit-vector. However, the discrete representation of such bit-vectors do not align well with downstream attention based modules so, instead of directly using one-hot vectors, the gumbel-softmax selects a value-specific encoding for each attribute. Thus, the resultant symbol vector is a composition of learnable latent encodings distinct to each attribute value. In implementation, SLM utilizes another zero-shot symbolic module (a spatial-softmax operation [41]) to extract positional attributes, such as the  $x$  and  $y$  position of the object, from the disentangled input vector.

#### 3.2.1 Action Conditioning

**ACTIONATTN** :  $\{\Lambda_1, \Lambda_2, \Lambda_k\} \times \{A_1, A_2, A_k\} \rightarrow \{\bar{\Lambda}_1, \bar{\Lambda}_2, \bar{\Lambda}_k\}$ : To predict the next state accurately, world models need to condition the state on the intended action. This conditioning is achieved by concatenating the action to the encoding. Ideally, if each entity occupies one slot and the slots have a canonical ordering, this conditioning can be achieved by simply concatenating the corresponding action to the corresponding encoding. However, the entities in a set structured representation do not have a fixed order. To find such a canonical ordering, we follow [44] in learning a permutation matrix between the actions and the slots and using the permutation matrix to reorder the slots

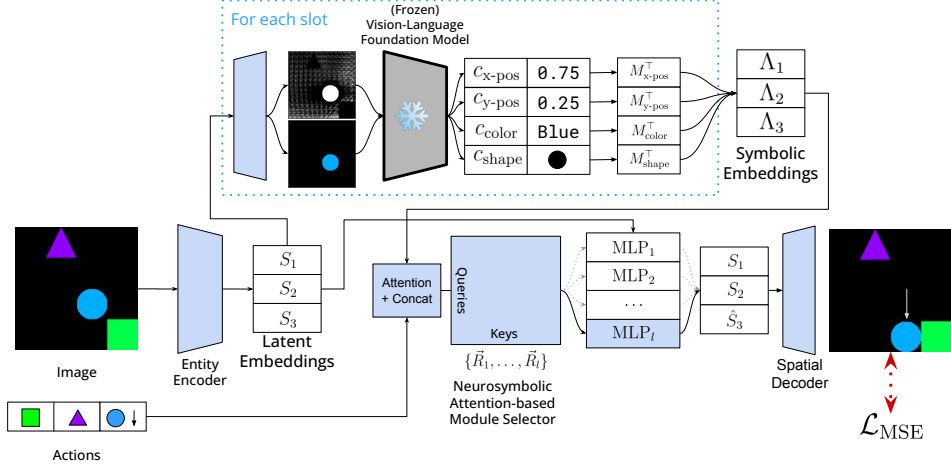


Figure 3: A single update step of COSMOS. The image  $I$  is fed through a slot-based autoencoder and a CLIP model to generate the slot encodings  $\{S_1, S_2, S_k\}$  and the symbol vectors  $\{\Lambda_1, \Lambda_2, \Lambda_k\}$ . The actions and the symbolic encoding are aligned and concatenated using a permutation equivariant action attention module, which are used to select the update rule to be applied to the slots. This figure depicts a single update step; in implementation, the update-select-transform step is repeated multiple times to model multi-object interactions.

and concatenate them with their respective actions. Attention, by construction, is equivariant with respect to slot order, which avoids the need to enforce a canonical ordering.

### 3.3 Transition Model

Monolithic transition models like GNNs and MLPs model every pairwise object interaction, which, in domains with sparse object interactions, leads to accumulating spurious correlations. Our modular transition model addresses this problem by selecting a relevant pairwise interaction and updating the encodings for those objects locally (following [9]). We model this selection process by computing key-query *neurosymbolic attention* between ordered symbolic and neural rule encodings to determine the most applicable rule-slot pair. As each entity is composed of shared symbol vectors, the dot-product activations between the symbolic encodings and the rule encodings remain consistent for objects with identical attributes. Next, we will discuss the mechanisms of module selection and transitions.

**MODULESELECTOR** :  $\{\bar{\Lambda}_1, \bar{\Lambda}_2, \bar{\Lambda}_k\} \times \{\vec{R}_1, \vec{R}_2, \vec{R}_l\} \rightarrow (p, c, r)$ : The goal of the selection process is to select the primary slot, the contextual slot (which the primary slot will be conditioned on), and the update function to model the interaction. Query-key attention [3] serves as the base mechanism we will be using to perform selections. We compute query-key attention between the rule encoding and the action-conditioned symbolic encoding. The naive algorithm to compute this selection will take  $O(k^2l)$  time, where  $k$  is the number of slots and  $l$  is the number of rules. In implementation, the selection of  $(r, p, c)$  can be reduced to a runtime of  $O(kl + k)$  by *partial application* of the query-key attention. This algorithm is presented in appendix section 2.

**MLPBANK** :  $i \rightarrow \text{MLP}_i$ : Our modular transition function comprises a set of rules  $\mathbf{R}_1, \dots, \mathbf{R}_n$ , with each rule defined as  $\mathbf{R}_i = (\vec{R}_i, \text{MLP}_i)$ . Here,  $\vec{R}_i$  is a learnable encoding, while  $\text{MLP}_i : S_p \times S_c \rightarrow S'_p$  represents a submodule that facilitates pairwise interactions between objects. Intuitively, each submodule is learning how a primary state changes conditioned on a secondary state. In theory, each update function can be customized for different problems. However, in this study, we employ multi-layered perceptrons for all rules.

## 4 Experiments

We demonstrate the effectiveness of COSMOS on the 2D Block pushing domain [9, 19, 21, 44] with scene composition, and two instances of object composition. We selected the 2D block pushing

Dataset	Model	3 objects			5 objects		
		MSE ↓	AE-MSE ↓	Eq.MRR ↑	MSE ↓	AE-MSE ↓	Eq.MRR ↑
OC (Sticky)	COSMOS	<b>4.23E-03</b>	<b>4.90E-04</b>	<b>1.20E-01</b>	<b>4.15E-03</b>	<b>1.68E-03</b>	<b>3.67E-01</b>
	ALIGNEDNPS	1.14E-02	7.72E-03	8.01E-02	6.07E-03	2.47E-03	3.62E-01
	GNN	7.94E-03	5.11E-03	6.03E-04	6.21E-03	2.73E-03	5.30E-04
OC (Team)	COSMOS	<b>4.60E-03</b>	<b>4.33E-04</b>	1.04E-01	<b>5.53E-03</b>	1.86E-03	2.86E-01
	ALIGNEDNPS	1.24E-02	8.36E-03	<b>1.75E-01</b>	9.64E-03	3.12E-03	<b>2.93E-01</b>
	GNN	8.92E-03	3.82E-03	7.16E-04	7.01E-03	<b>1.62E-03</b>	5.46E-04
SC	COSMOS	<b>7.66E-04</b>	<b>6.34E-05</b>	2.99E-01	<b>4.08E-04</b>	<b>2.92E-06</b>	3.03E-01
	ALIGNEDNPS	3.51E-03	2.69E-03	2.97E-01	2.45E-03	1.22E-03	3.19E-01
	GNN	9.89E-03	1.03E-02	<b>5.50E-01</b>	1.20E-02	1.28E-02	<b>5.25E-01</b>

Table 1: Evaluation results on the 2D block pushing domain for scene composition (SC) and object composition (OC) averaged across three seeds. We report next-state reconstruction error (MSE), autoencoder reconstruction error (AE-MSE), and the equivariant mean reciprocal rank (Eq.MRR) for three transition models: our model (COSMOS), an improved version of [9] (ALIGNEDNPS), and a reimplementaion of [44] (GNN). Our model (COSMOS) achieves best next-state reconstructions for all datasets.

domain as it is a widely-adopted and well-studied benchmark in the community. Notably, even in this synthetic domain, our instances of compositional generalization proved challenging to surpass for baseline models, underscoring the difficulty of the problem.

**2D Block Pushing Domain:** The 2D block pushing domain [19, 21] is a two-dimensional environment that necessitates dynamic and perceptual reasoning. Figure 5 presents an overview of this domain. All objects have four attributes: color ( $\Lambda^{C_{\text{color}}}$ ), shape ( $\Lambda^{C_{\text{shape}}}$ ),  $x$  position ( $\Lambda^{C_{x\text{-pos}}}$ ), and  $y$  position ( $\Lambda^{C_{y\text{-pos}}}$ ). Objects can be pushed in one of the four cardinal directions (North-East-South-West). Heavier objects can push lighter objects, but not the other way around. The weight of the object depends on the shape attribute. At each step, the agent observes an image of size  $3 \times 224 \times 224$  with  $k$  objects and an action pushing one of the objects. This action is chosen from a uniform random distribution. The goal is for the agent to capture the dynamics of object movement. Furthermore, while there are  $n = |A_{\text{color}}| \times |A_{\text{shape}}|$  unique objects in total, only  $k < n$  objects are allowed to co-occur in a realized scene.

**Dataset Setup:** We adapt the methodology from [21, 44] with minor changes. For scene compositions (SC), we construct training and testing to have unique object combinations. In object composition (OC), objects with matching attributes exhibit identical dynamics. Two specific cases are explored: Team Composition (OC-Team) where dynamics are shared based on color, and Sticky Composition (OC-Sticky) where dynamics are shared based on color and adjacency. Further details are in the appendix (Section A.1). Our data generation methodology ensures that the compound distribution is disjoint, while the atom distribution remains consistent across datasets, i.e.  $\mathcal{F}_C(\mathcal{D}_{\text{train}}) \cap \mathcal{F}_C(\mathcal{D}_{\text{eval}}) = \emptyset$  and  $\mathcal{F}_A(\mathcal{D}_{\text{train}}) = \mathcal{F}_A(\mathcal{D}_{\text{eval}})$ . The difficulty of the domain can be raised by increasing the number of objects. We sample datasets for 3 and 5 objects.

**Evaluation:** We compare against past works in compositional world modeling with publically available codebases at the time of writing. For the block pushing domain, we compare against Homomorphic world models (GNN) [44] and NPS [9] with modifications to ensure that the actions are aligned with the slots (ALIGNEDNPS). The latter is equivalent to an ablation of COSMOS without the symbolic labelling module. For compositional world modeling, we analyzed next-state predictions using mean squared error (MSE), current-state reconstructions using auto-encoder mean squared error (AE-MSE), and latent state separation using (MRR) following previous work [9, 21, 44]. Recognizing limitations in existing MRR calculation, we introduce the Equivariant MRR (Eq.MRR) metric, which accounts for different slot orders when calculating the MRR score. More details can be found in the appendix Section A.3.

**Results:** Results are presented in Table 2. First, we find that COSMOS achieves the best next state prediction performance (MSE) on all benchmarks. Moving from scene composition to object composition datasets shows a drop in performance, underscoring the complexity of the task. Surprisingly, there is less than expected performance degradation moving from the three object to five object domain. We attribute this to the nature of the block pushing domain and the choice of loss



function. MSE loss measures the pixel error between the predicted and next image. As the density of objects in the image increases, the reconstruction target becomes more informative, encouraging better self-correction, and hence more efficient training.

Second, we observe that, without neurosymbolic grounding, the slot autoencoder’s ability to encode and decode images degrades as the world model training progresses. This suggests that neurosymbolic grounding guards against auto-encoder representation collapse.

Finally, we do not notice a consistent pattern in the Equivariant MRR scores between models. First, all models tend to exhibit a higher Eq.MRR score in the five object environments. However, in many cases, models with high Eq.MRR score also have underperforming autoencoders. For instance, in the five object scene composition case, the GNN exhibits a high Eq.MRR score yet simultaneously has the worst autoencoder reconstruction error. We notice this happens when the model suffers a partial representation collapse (overfitting to certain color, shapes combination seen during training). This maps many slot encodings to the same neighborhood in latent space; making it easier to retrieve similar encodings, boosting the MRR score. Given these observations, we conclude that MRR might not be an optimal indicator of a model’s downstream utility. For a comprehensive assessment of downstream utility, we turn to the methodology outlined by [36], applying the models to a downstream planning task.

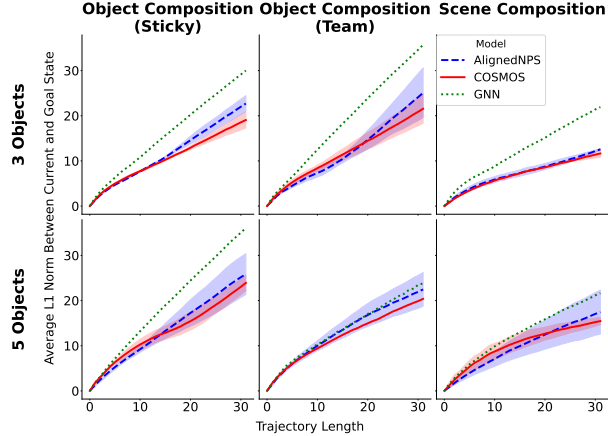


Figure 4: Downstream utility of different world models using a greedy planner. The graph follows the average L1 error between the chosen next state and the ground truth next state as a function of the number of steps the model takes. A lower L1 error indicates better performance. COSMOS (in red) achieves the best performance.

**Downstream Utility:** We evaluate the downstream utility of all world models using a simple planning task in 2D shapeworld environments. Our method, inspired by [36], involves using a greedy planner that acts based on the Hungarian distance between the predicted and goal states. Due to the compounding nature of actions over a trajectory, there is an observed divergence from the ground truth the deeper we get into the trajectory. We run these experiments on our test dataset and average the scores at each trajectory depth. We showcase results in Figure 4. Our model (COSMOS) shows the most consistency and least deviation from the goal state in all datasets, which suggests that neurosymbolic grounding helps improve the downstream efficacy of world models. More details can be found in appendix section A.4.

## 5 Related Work

**Object-Oriented World Models:** Object-oriented world models [9, 21, 34, 36, 44] are constructed to learn structured latent spaces that facilitate efficient dynamics prediction in environments that can be decomposed into unique objects. We highlight two primary themes in this domain.

*Interaction Modeling and Modularity in Representations:* [21] offers a contrastive world modeling technique using graph neural networks on an object-factored representation. However, GNNs may introduce compounding errors in sparse interaction domains. Addressing this, [10] introduces neural production systems (NPS) for modeling sparse interactions, akin to repeated dynamic instantiation GNN edge instantiation. COSMOS is influenced by the NPS architecture, with distinctions highlighted in Figure 2. In parallel, [4] studies a hierarchical abstraction for world models, decomposing slots into a (dynamics relevant) state vector and a (dynamics invariant) type vector, with dynamics prediction focusing on the state vector. COSMOS’s symbolic abstraction is a generalization of this abstraction. Instead of maintaining a single “type vector”, we maintain a set of learnable symbol



vectors and select a relevant subset for each entity. This allows COSMOS to naturally discover global and local invariances, utilizing them to route latent encodings (akin to “state vectors”) to appropriate transition modules.

*Compositional Generation and Equivariance in World Models:* Equivariant neural networks harness group symmetries for efficient learning [6, 7, 26, 28, 37]. In the context of CG, [35] investigates constructing equivariant neural networks within the MDP state-action space. [44] establishes a connection between homomorphic MDPs and compositional generalization, expressing CG as a symmetry group of equivariance to object permutations and developing a world model equivariant to object permutation (using action attention). COSMOS adopts this idea, but integrates a modular transition model that also respects permutation equivariance in slot order.

**Vision-grounded Neurosymbolic Learning:** Prior work in neurosymbolic learning has demonstrated that symbolic grounding helps facilitate domain generalization and data efficiency [1, 2, 16, 24, 29, 30, 42, 43]. The interplay between neural and symbolic encodings in these works can be abstracted into three categories: (1) scaffolding perceptual inputs with precomputed symbolic information for downstream prediction [2, 8, 16, 24, 33], (2) learning a symbolic abstraction from a perceptual input useful for downstream prediction [32], and (3) jointly learning a neural and symbolic encodings leveraged for prediction [43]. Our approach aligns most closely with the third category. While [43] combine neural and symbolic encoders in a VAE setting, highlighting the regularization advantages of symbols for unsupervised clustering, they rely on a program synthesizer to search for symbolic transformations in a DSL—introducing scalability and expressiveness issues. COSMOS also crafts a neurosymbolic encoding, but addresses scalability and expressiveness concerns of program synthesis by using a foundation model to generate the symbolic encodings.

**Foundation Models as Symbol Extractors:** Many works employ foundation models to decompose complex visual reasoning tasks [11, 25, 38]. [16, 39] decompose natural language instructions into executable programs using a Code LLM for robotic manipulation and 3D understanding. Notably, [31] uses Code LLMs to decomposes natural language queries to API calls in a library of pretrained models. Such approaches necessitate hand-engineering the API to be expressive enough to generalize to all attributes in a domain. COSMOS builds upon the idea of using compositionality of symbols to execute parameterized modules but sidesteps the symbolic decomposition bottleneck by parsimoniously using the symbolic encodings only for selecting representative encodings. I.e., COSMOS does not need its symbols to learn perfect reconstructions. The symbolic encoding is only used for selecting modules, while the neural encoding can learn fine-grained dynamics-relevant attributes that may not be known ahead of time. Furthermore, to the best of our knowledge, COSMOS is the first work to leverage vision-language foundation models for compositional world modeling.

## 6 Conclusion

We have presented COSMOS, a new neurosymbolic approach for compositionally generalizable world modeling. Our two key findings are that annotating entities with symbolic attributes can help with CG and that it is possible to get these symbols “for free” from foundation models. We have considered two definitions of CG — one new to this paper — and show that: (i) CG world modeling still has a long way to go regarding performance, and (ii) neurosymbolic grounding helps enhance CG.

Our work here aimed to give an initial demonstration of how foundation models can help compositional world modeling. However, foundation models are advancing at a breathtaking pace. Future work could extend our framework with richer symbolic representations obtained from more powerful vision-language or vision-code models. Also, our neurosymbolic attention mechanism could be naturally expanded into a neurosymbolic transformer. Finally, the area of compositional world modeling needs more benchmarks and datasets. Future work should take on the design of such artifacts with the goal of developing generalizable and robust world models.

## 7 Acknowledgements

Research supported by The NSF National AI Institute for Foundations of Machine Learning (IFML), ARO award #W911NF-21-1-0009, and DARPA award #HR00112320018.

## References

- [1] Jacob Andreas, Marcus Rohrbach, Trevor Darrell, and Dan Klein. Learning to compose neural networks for question answering. *arXiv preprint arXiv:1601.01705*, 2016.
- [2] Jacob Andreas, Marcus Rohrbach, Trevor Darrell, and Dan Klein. Neural module networks. In *Proceedings of the IEEE conference on computer vision and pattern recognition*, pages 39–48, 2016.
- [3] Dzmitry Bahdanau, Kyunghyun Cho, and Yoshua Bengio. Neural machine translation by jointly learning to align and translate. In *ICLR*, 2015.
- [4] Michael Chang, Alyssa L. Dayan, Franziska Meier, Thomas L. Griffiths, Sergey Levine, and Amy Zhang. Hierarchical abstraction for combinatorial generalization in object rearrangement. In *The Eleventh International Conference on Learning Representations, ICLR 2023, Kigali, Rwanda, May 1-5, 2023*. OpenReview.net, 2023.
- [5] Michael Chang, Tom Griffiths, and Sergey Levine. Object representations as fixed points: Training iterative refinement algorithms with implicit differentiation. *Advances in Neural Information Processing Systems*, 35:32694–32708, 2022.
- [6] Taco Cohen and Max Welling. Group equivariant convolutional networks. In *International conference on machine learning*, pages 2990–2999. PMLR, 2016.
- [7] Taco S Cohen and Max Welling. Steerable cnns. *arXiv preprint arXiv:1612.08498*, 2016.
- [8] Kevin Ellis, Daniel Ritchie, Armando Solar-Lezama, and Josh Tenenbaum. Learning to infer graphics programs from hand-drawn images. In *Advances in neural information processing systems*, pages 6059–6068, 2018.
- [9] Anirudh Goyal, Aniket Didolkar, Nan Rosemary Ke, Charles Blundell, Philippe Beaudoin, Nicolas Heess, Michael Mozer, and Yoshua Bengio. Neural production systems. *Neural Information Processing Systems*, 2021.
- [10] Anirudh Goyal, Aniket Didolkar, Nan Rosemary Ke, Charles Blundell, Philippe Beaudoin, Nicolas Heess, Michael C Mozer, and Yoshua Bengio. Neural production systems. *Advances in Neural Information Processing Systems*, 34:25673–25687, 2021.
- [11] Tanmay Gupta and Aniruddha Kembhavi. Visual programming: Compositional visual reasoning without training. In *Proceedings of the IEEE/CVF Conference on Computer Vision and Pattern Recognition*, pages 14953–14962, 2023.
- [12] David Ha and Jürgen Schmidhuber. World models. *arXiv preprint arXiv:1803.10122*, 2018.
- [13] Danijar Hafner, Jurgis Pasukonis, Jimmy Ba, and Timothy Lillicrap. Mastering diverse domains through world models. *arXiv preprint arXiv:2301.04104*, 2023.
- [14] Stevan Harnad. The symbol grounding problem. *Physica D: Nonlinear Phenomena*, 42(1-3):335–346, 1990.
- [15] Kaiming He, Xiangyu Zhang, Shaoqing Ren, and Jian Sun. Deep residual learning for image recognition. In *Proceedings of the IEEE conference on computer vision and pattern recognition*, pages 770–778, 2016.
- [16] Joy Hsu, Jiayuan Mao, and Jiajun Wu. Ns3d: Neuro-symbolic grounding of 3d objects and relations. In *Proceedings of the IEEE/CVF Conference on Computer Vision and Pattern Recognition*, pages 2614–2623, 2023.
- [17] Eric Jang, Shixiang Gu, and Ben Poole. Categorical reparameterization with gumbel-softmax. *arXiv preprint arXiv:1611.01144*, 2016.
- [18] Baoxiong Jia, Yu Liu, and Siyuan Huang. Improving object-centric learning with query optimization. In *The Eleventh International Conference on Learning Representations*, 2022.
- [19] Nan Rosemary Ke, Aniket Didolkar, Sarthak Mittal, Anirudh Goyal, Guillaume Lajoie, Stefan Bauer, Danilo Rezende, Yoshua Bengio, Michael Mozer, and Christopher Pal. Systematic evaluation of causal discovery in visual model based reinforcement learning. *arXiv preprint arXiv:2107.00848*, 2021.
- [20] Daniel Keysers, Nathanael Schärli, Nathan Scales, Hylke Buisman, Daniel Furrer, Sergii Kashubin, Nikola Momchev, Danila Sinopalnikov, Lukasz Stafiniak, Tibor Tihon, Dmitry

- Tsarkov, Xiao Wang, Marc van Zee, and Olivier Bousquet. Measuring compositional generalization: A comprehensive method on realistic data. In *International Conference on Learning Representations*, 2020.
- [21] Thomas Kipf, Elise Van der Pol, and Max Welling. Contrastive learning of structured world models. *arXiv preprint arXiv:1911.12247*, 2019.
  - [22] Alexander Kirillov, Eric Mintun, Nikhila Ravi, Hanzi Mao, Chloe Rolland, Laura Gustafson, Tete Xiao, Spencer Whitehead, Alexander C. Berg, Wan-Yen Lo, Piotr Dollár, and Ross Girshick. Segment anything. *arXiv:2304.02643*, 2023.
  - [23] Francesco Locatello, Dirk Weissenborn, Thomas Unterthiner, Aravindh Mahendran, Georg Heigold, Jakob Uszkoreit, Alexey Dosovitskiy, and Thomas Kipf. Object-centric learning with slot attention. *Advances in Neural Information Processing Systems*, 33:11525–11538, 2020.
  - [24] Jiayuan Mao, Xiuming Zhang, Yikai Li, William T Freeman, Joshua B Tenenbaum, and Jiajun Wu. Program-guided image manipulators. In *Proceedings of the IEEE International Conference on Computer Vision*, pages 4030–4039, 2019.
  - [25] Nihal V Nayak, Peilin Yu, and Stephen H Bach. Learning to compose soft prompts for compositional zero-shot learning. *arXiv preprint arXiv:2204.03574*, 2022.
  - [26] Jung Yeon Park, Ondrej Biza, Linfeng Zhao, Jan Willem van de Meent, and Robin Walters. Learning symmetric embeddings for equivariant world models. *arXiv preprint arXiv:2204.11371*, 2022.
  - [27] Alec Radford, Jong Wook Kim, Chris Hallacy, Aditya Ramesh, Gabriel Goh, Sandhini Agarwal, Girish Sastry, Amanda Askell, Pamela Mishkin, Jack Clark, et al. Learning transferable visual models from natural language supervision. In *International conference on machine learning*, pages 8748–8763. PMLR, 2021.
  - [28] Balaraman Ravindran. *An algebraic approach to abstraction in reinforcement learning*. University of Massachusetts Amherst, 2004.
  - [29] Ameesh Shah, Eric Zhan, Jennifer J Sun, Abhinav Verma, Yisong Yue, and Swarat Chaudhuri. Learning differentiable programs with admissible neural heuristics. In *Advances in Neural Information Processing Systems*, 2020.
  - [30] Jennifer J Sun, Ann Kennedy, Eric Zhan, David J Anderson, Yisong Yue, and Pietro Perona. Task programming: Learning data efficient behavior representations. In *Proceedings of the IEEE/CVF Conference on Computer Vision and Pattern Recognition*, pages 2876–2885, 2021.
  - [31] Dídac Surís, Sachit Menon, and Carl Vondrick. Vipergpt: Visual inference via python execution for reasoning. *arXiv preprint arXiv:2303.08128*, 2023.
  - [32] Hao Tang and Kevin Ellis. From perception to programs: regularize, overparameterize, and amortize. In *International Conference on Machine Learning*, pages 33616–33631. PMLR, 2023.
  - [33] Lazar Valkov, Dipak Chaudhari, Akash Srivastava, Charles Sutton, and Swarat Chaudhuri. Houdini: Lifelong learning as program synthesis. In *Advances in Neural Information Processing Systems*, pages 8701–8712, 2018.
  - [34] Elise Van der Pol, Thomas Kipf, Frans A Oliehoek, and Max Welling. Plannable approximations to mdp homomorphisms: Equivariance under actions. *arXiv preprint arXiv:2002.11963*, 2020.
  - [35] Elise Van der Pol, Daniel Worrall, Herke van Hoof, Frans Oliehoek, and Max Welling. Mdp homomorphic networks: Group symmetries in reinforcement learning. *Advances in Neural Information Processing Systems*, 33:4199–4210, 2020.
  - [36] Rishi Veerapaneni, John D. Co-Reyes, Michael Chang, Michael Janner, Chelsea Finn, Jiajun Wu, Joshua Tenenbaum, and Sergey Levine. Entity abstraction in visual model-based reinforcement learning. In Leslie Pack Kaelbling, Danica Kragic, and Komei Sugiura, editors, *Proceedings of the Conference on Robot Learning*, volume 100 of *Proceedings of Machine Learning Research*, pages 1439–1456. PMLR, 30 Oct–01 Nov 2020.
  - [37] Robin Walters, Jinxi Li, and Rose Yu. Trajectory prediction using equivariant continuous convolution. *arXiv preprint arXiv:2010.11344*, 2020.

- [38] Guanzhi Wang, Yuqi Xie, Yunfan Jiang, Ajay Mandlekar, Chaowei Xiao, Yuke Zhu, Linxi Fan, and Anima Anandkumar. Voyager: An open-ended embodied agent with large language models. *arXiv preprint arXiv:2305.16291*, 2023.
- [39] Renhao Wang, Jiayuan Mao, Joy Hsu, Hang Zhao, Jiajun Wu, and Yang Gao. Programmatically grounded, compositionally generalizable robotic manipulation. *arXiv preprint arXiv:2304.13826*, 2023.
- [40] Nicholas Watters, Loic Matthey, Matko Bosnjak, Christopher P Burgess, and Alexander Lerchner. Cobra: Data-efficient model-based rl through unsupervised object discovery and curiosity-driven exploration. *arXiv preprint arXiv:1905.09275*, 2019.
- [41] Nicholas Watters, Loic Matthey, Christopher P Burgess, and Alexander Lerchner. Spatial broadcast decoder: A simple architecture for learning disentangled representations in vaes. *arXiv preprint arXiv:1901.07017*, 2019.
- [42] Kexin Yi, Jiajun Wu, Chuang Gan, Antonio Torralba, Pushmeet Kohli, and Josh Tenenbaum. Neural-symbolic vqa: Disentangling reasoning from vision and language understanding. *Advances in neural information processing systems*, 31, 2018.
- [43] Eric Zhan, Jennifer J. Sun, Ann Kennedy, Yisong Yue, and Swarat Chaudhuri. Unsupervised learning of neurosymbolic encoders. *CoRR*, abs/2107.13132, 2021.
- [44] Linfeng Zhao, Lingzhi Kong, Robin Walters, and Lawson LS Wong. Toward compositional generalization in object-oriented world modeling. In *International Conference on Machine Learning*, pages 26841–26864. PMLR, 2022.

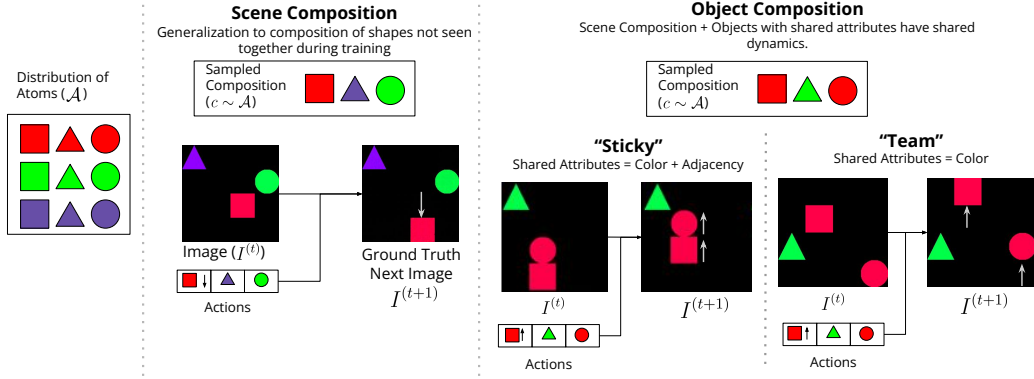


Figure 5: Overview of types of compositions studied. Scene composition (left) necessitates learning a world model that is equivariant to object replacement. Object compositions (right) necessitates learning the properties of scene composition as well as additional constraints where objects with shared attributes also have shared dynamics. We study two instantiations of shared attributes sets: “Sticky” and “Team”. Details on these instantiations are given in Appendix A.1.

## A Appendix

The Appendix is divided into five sections. Section A.1 surveys the types of compositions we study in detail, Section A.2 introduces a faster algorithm used in implementation for module selection, Section A.3 outlines experiment details and, notably, presents justification for the Equivariant MRR metric employed to study encoding separation, Section A.4 presents details of how the downstream planning experiments were conducted, and Section A.5 showcases qualitative results on a randomly sampled subset of five-object state-action pairs.

### A.1 Types of Compositions

**Scene Composition:** Scene composition (Figure 5) necessitates learning a world model that is equivariant to object replacement. The dynamics of the environment depends on which objects are present in the scene.

**Object Composition:** Object composition (Figure 5) necessitates learning all the properties present in scene composition. Additionally, in object composition, the composition is determined by constraints placed on observable attributes of individual objects. For instance, in Sticky block pushing (Fig 5), the scene is constrained so that two objects start out with the same color adjacent to each other; and an action on one object moves all objects of the same color with it. This gives the appearance of two objects being stuck to each other. At test time, the objects stuck together change. Sticky block pushing demonstrates compositionality constraints based on two attributes: position and color. In the team block pushing (Figure 5), we relax the adjacency constraint in the sticky block pushing domain. An action on any object also moves other objects of the same color. This allows us to study whether the adjacency constraint places a larger burden on dynamics learning than the color constraint.

### A.2 Transition Algorithm

NPS [9] necessitates selecting a primary slot ( $p$ ) to be modified, a contextual slot ( $c$ ), and a rule ( $r$ ) to modify the primary slot in the presence of the contextual slot. The naive algorithm to compute this tuple has a runtime of  $O(k^2l)$  where  $k$  is the number of slots and  $l$  is the number of rules. However, in implementation, the selection of  $(r, p, c)$  can be reduced to a runtime of  $O(kl + k)$  by *partial application* of the query-key attention. This is achieved by selecting the primary slot  $p$  and  $\text{MLP}_{i_p}$ , partially transforming  $S_p$  using a partial transition module  $\text{MLP}_{(i, \text{left})}$ , selecting the contextual slot  $c$ , and performing a final transformation of  $\text{MLP}_{(i, \text{left})}(S_p)$  with  $S_c$  using  $\text{MLP}_{(i, \text{right})}$ . Algorithm 2 presents this faster algorithm.

**Algorithm 2** Faster Transition Algorithm. This algorithm has a faster runtime than the one presented in the manuscript. The main difference is that the transition step is bifurcated into two parts, reducing the runtime of the selection from  $O(k^2l)$  to  $O(kl + k)$  where  $k$  is the number of slots and  $l$  is the number of rules.

---

```

1: function TRANSITION(Key= $\{\bar{\Lambda}_1, \bar{\Lambda}_2, \bar{\Lambda}_k\}$ , Query= $\{\vec{R}_1, \vec{R}_2, \vec{R}_l\}$ , Value= $\{S_1, S_2, S_k\}$ )
2:    $\mathbf{A}^* \leftarrow \text{GumbelSoftmax}(\text{KQAttention}(\text{key}=\{\bar{\Lambda}_1, \bar{\Lambda}_2, \bar{\Lambda}_k\}, \text{query}=\{\vec{R}_1, \vec{R}_2, \vec{R}_l\}))$ 
3:    $p, r \leftarrow \text{argmax}(\mathbf{A}^*, \text{axis} = \text{'all'})$ 
4:    $S^* \leftarrow \text{LeftMLPBank}[r](\text{concat}(S_p, \vec{R}_r))$ 
5:    $\mathbf{A}_2^* \leftarrow \text{GumbelSoftmax}(\text{KQAttention}(\text{key}=\{\bar{\Lambda}_1, \bar{\Lambda}_2, \bar{\Lambda}_k\}, \text{query}=\{S^*, S^*, S^*\}))$ 
6:    $c, _ \leftarrow \text{argmax}(\mathbf{A}_2^*, \text{axis} = \text{'all'})$ 
7:    $S_2^* \leftarrow \text{RightMLPBank}[r](\text{concat}(S_c, S^*))$ 
8:   return  $S_2^*$ 

```

---

### A.3 Evaluation Procedure

**Dataset Generation:** To generate each dataset, we first create a scene configuration file that pre-describes the permissible shapes and colors for objects within a given dataset. The scene configuration ensures that  $\mathcal{F}_C(\mathcal{D}_{train}) \cap \mathcal{F}_C(\mathcal{D}_{eval}) = \emptyset$ . Next, we sample  $\mathcal{D}_{train}$  and  $\mathcal{D}_{eval}$  from the permissible scenes. Each dataset is a trajectory of state-action pairs, where the state is the image of the shape  $3 \times 224 \times 224$  and the action is a vector, factorized by object ID (Object x North-East-South-West). Overall, we generate 3000 trajectories of length 32 each where the actions are sampled from a random uniform distribution. Our domain is equivalent to the observed weighted shapes setup studied in [19] with a compositionality constraint where the weight of the objects depend only on the shapes.

**Baselines:** We compare against past works in compositional world modeling with publicly available codebases at the time of writing. For the block pushing domain, we compare against Homomorphic world models (GNN) [44] and an ablation of our model without symbols (ALIGNEDNPS). HOWM uses a slot autoencoder, an action attention module and a GNN for modeling transitions. It requires a two-step training process: first warm starting the slot-autoencoder and then training the action attention model and GNN with an equivariant contrastive loss (Hungarian matching loss). NPS uses a slot autoencoder for modeling perceptions and a NPS module for modeling transitions. The pipeline is trained end to end with contrastive loss. We use action attention with NPS as well. For both models, we weren't able to reproduce the results using the provided codebases due to issues in training robust perception models for large images ( $3 \times 224 \times 224$ ). To ensure a fair comparison, and since both these methods are agnostic to the perception model, we opt to reimplement the core ideas for both these models and use the same fine-tuned perception model for all models.

**Evaluation Procedure:** We evaluate all models on a single 48 GB NVIDIA A40 GPU with a (maximum possible) batch size of 64 for 50 epochs for three random seeds. Contrastive learning necessitates a large batch size to ensure a diverse negative sampling set. As a result, the small batch size made contrastive learning challenging in our domain. To ensure a fair comparison, we report results for all models trained using reconstruction loss. We first train the slot autoencoder (ENTITYEXTRACTOR and SPATIALDECODER) until the model shows no training improvement for 5 epochs. This is sufficient to learn slot autoencoders with near-perfect state reconstructions. All

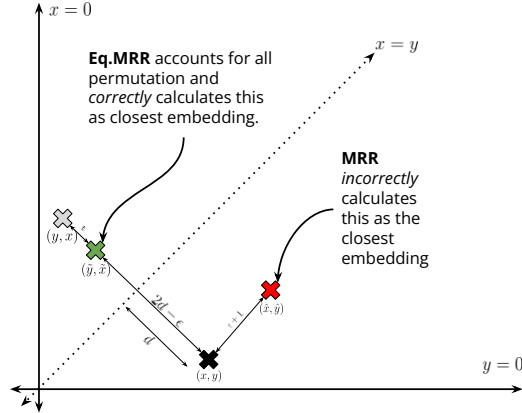


Figure 6: Intuition for shortcomings of MRR when number of slots  $k = 2$  and  $d_{slot} = 1$ . The MRR metric incorrectly finds a point  $(\hat{x}, \hat{y})$  that is  $\epsilon + 1$  units away from  $(x, y)$  while Equivariant MRR considers all possible permutations and finds a point  $(\tilde{y}, \tilde{x})$  that is  $\epsilon$  units away from  $(y, x)$  and, in turn, closer to  $(x, y)$  than  $(\hat{x}, \hat{y})$ .

Dataset	Model	3 objects			5 objects		
		MSE ↓	AE-MSE ↓	Eq.MRR ↑	MSE ↓	AE-MSE ↓	Eq.MRR ↑
OC (Sticky)	COSMOS	<b>4.23E-03 +/- 1.49E-04</b>	<b>4.90E-04 +/- 1.03E-04</b>	<b>1.20E-01 +/- 2.05E-02</b>	<b>4.15E-03 +/- 3.21E-03</b>	<b>1.68E-03 +/- 1.48E-03</b>	<b>3.67E-01 +/- 7.73E-02</b>
	ALIGNEDNPS	1.14E-02 +/- 9.89E-04	7.72E-03 +/- 1.21E-03	8.01E-02 +/- 6.79E-02	6.07E-03 +/- 8.30E-04	2.47E-03 +/- 3.60E-04	3.62E-01 +/- 1.81E-02
	GNN	7.94E-03 +/- 5.47E-03	5.11E-03 +/- 4.94E-03	6.03E-04 +/- 1.02E-04	6.21E-03 +/- 1.26E-03	2.73E-03 +/- 1.27E-03	5.30E-04 +/- 5.15E-05
OC (Team)	COSMOS	<b>4.60E-03 +/- 2.32E-03</b>	<b>4.33E-04 +/- 1.58E-04</b>	1.04E-01 +/- 3.19E-02	<b>5.53E-03 +/- 1.95E-03</b>	1.86E-03 +/- 1.61E-03	2.86E-01 +/- 4.32E-02
	ALIGNEDNPS	1.24E-02 +/- 4.11E-04	8.36E-03 +/- 6.78E-04	<b>1.75E-01 +/- 2.68E-02</b>	9.64E-03 +/- 1.95E-04	3.12E-03 +/- 6.07E-04	<b>2.93E-01 +/- 2.02E-02</b>
	GNN	8.92E-03 +/- 6.05E-03	3.82E-03 +/- 3.64E-03	7.16E-04 +/- 1.09E-04	7.01E-03 +/- 9.81E-04	<b>1.62E-03 +/- 1.04E-03</b>	5.46E-04 +/- 1.37E-04
SC	COSMOS	<b>7.66E-04 +/- 4.08E-04</b>	<b>6.34E-05 +/- 2.01E-05</b>	2.99E-01 +/- 2.85E-02	<b>4.08E-04 +/- 4.68E-06</b>	<b>2.92E-06 +/- 6.34E-07</b>	3.03E-01 +/- 3.88E-02
	ALIGNEDNPS	3.51E-03 +/- 6.30E-04	2.69E-03 +/- 6.89E-05	2.97E-01 +/- 7.99E-02	2.45E-03 +/- 3.47E-04	1.22E-03 +/- 9.06E-04	3.19E-01 +/- 1.01E-01
	GNN	9.89E-03 +/- 5.77E-03	1.03E-02 +/- 5.44E-03	<b>5.50E-01 +/- 5.18E-01</b>	1.20E-02 +/- 1.13E-02	1.28E-02 +/- 1.08E-02	<b>5.25E-01 +/- 2.67E-01</b>

Table 2: Evaluation results on the 2D block pushing domain for scene composition (SC) and object composition (OC) averaged across three seeds. This table includes standard deviation numbers as well. Our model (COSMOS) achieves best next-state reconstructions for all datasets.

transition models are initialized with the same slot-autoencoder and are optimized to minimize a mixture of the autoencoder reconstruction loss and the next-state reconstruction loss. For compositional world modeling, we are interested in two aspects of model performance: next-state predictions and separation between latent states. We evaluate next-state predictions on all models using the mean squared error (MSE) between the predicted next image and the ground truth next image in the experience buffer. We also measure the performance of the autoencoder on reconstructing the current state by calculating the slot-autoencoder mean squared error (AE-MSE). Generally, training world models improves the perception model’s ability to reconstruct states as well. We also evaluate the separability of the learned latent encodings. This is done by measuring the L2 distance between the predicted next slot encodings and the ground-truth next slot encodings obtained from the encoder and using information theoretic measures such as mean reciprocal rank (MRR) to measure similarity. Notably, the MRR computation in previous work does not account for the non-canonical order of slots, causing higher L2 distance and, consecutively, higher MRR scores when the target and predicted slots have different orderings. The core issue here is that MRR computation, as used in previous works, fixed the order of the slots before calculating L2 distance. This ignored  $k! - 1$  possible orderings where a closer target encoding could be found. To rectify this, we propose a new metric, Equivariant MRR (Eq.MRR), which uses the minimum L2 distance among all permutations of slot encodings to calculate mean reciprocal rank. This metric ensures that the latent slot encodings are not penalized for having different slot orders. Figure 6 presents an illustration of the shortcomings of MRR on a simple example. This limitation is characteristic of algorithms which do not align the slots to a canonical slot ordering. In practice, we observe that the Equivariant MRR is always lower than or equal to the MRR.

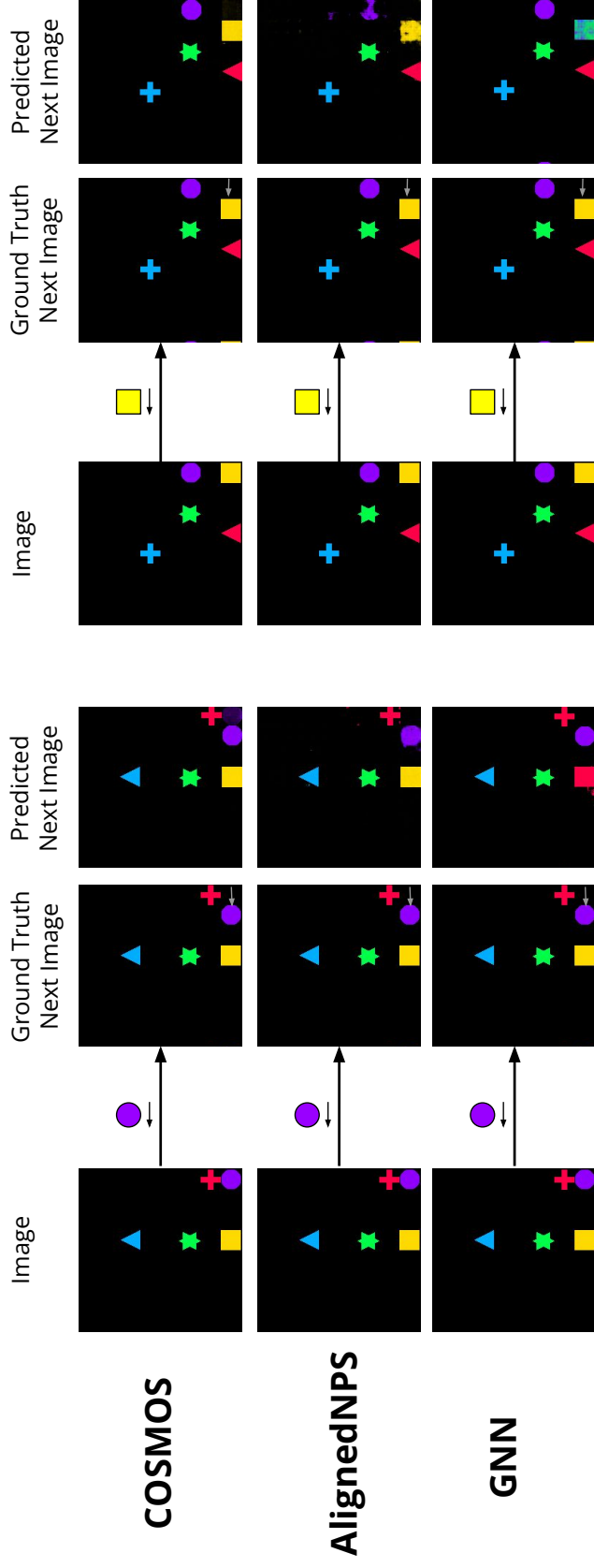
#### A.4 Downstream Evaluation Setup

Following [36], we use a greedy planner that chooses the action that minimizes the Hungarian distance between the current and the goal state. These actions are applied  $t - 1$  times over a trajectory of length  $t$ , with the output from the world model at the  $(d - 1)$ -th step becoming the state for step  $d$  in the trajectory. Due to this compounding nature, we see an increased divergence from the ground truth as we get deeper into the trajectory. At each step  $d$  in the trajectory, the accuracy of the world model is evaluated as the L1 error of the difference between the current ground truth and predicted states in the form of their  $xy$ -coordinates. These  $xy$ -coordinates are initialized for each object to the origin and updated with every action taken by the corresponding rule. For example, after one step, if the ground truth moves an object to the east, but the planner chooses to move the same object to the west, then the distance between the two states would be 2. We run these experiments for the 500 trajectories of length  $t = 32$  in our test dataset and average the scores at each trajectory depth. We showcase results in Figure 4. Our model (COSMOS) shows the most consistency and least deviation from the goal state in all datasets, which suggests that neurosymbolic grounding helps improve the downstream efficacy of world models.

#### A.5 Qualitative Results



## Scene Composition



## Object Composition (Sticky Shapeworld)

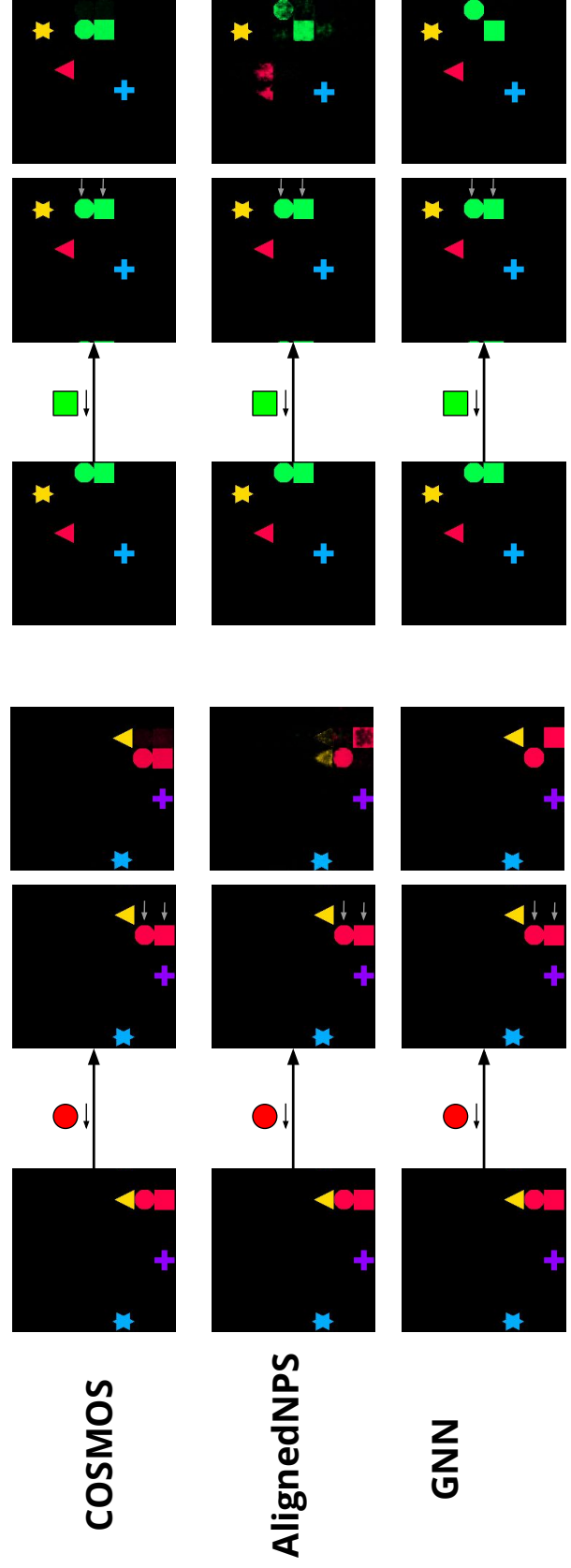


Figure 7: Qualitative outputs on randomly chosen state-action pairs for all baselines. We show two samples for each experiment and dataset type with 5 objects. Color is shown for illustrative purposes only; in implementation, the action conditioning does not carry any information about color.